THE EUROPEAN
PHYSICAL JOURNAL A

Femtoscopic study on DD^* and $D\bar{D}^*$ interactions for T_{cc} and $X(3872)$

Yuki Kamiya[1,2,a] ⬤, Tetsuo Hyodo[2,3,b] ⬤, Akira Ohnishi[4,c] ⬤

[1] Helmholtz Institut für Strahlen- und Kernphysik and Bethe Center for Theoretical Physics, Universität Bonn, 53115 Bonn, Germany
[2] RIKEN Interdisciplinary Theoretical and Mathematical Science Program (iTHEMS), Wako 351-0198, Japan
[3] Department of Physics, Tokyo Metropolitan University, Hachioji 192-0397, Japan
[4] Yukawa Institute for Theoretical Physics, Kyoto University, Kyoto 606-8502, Japan

Abstract We investigate DD^* and $D\bar{D}^*$ momentum correlations in high-energy collisions to elucidate the nature of T_{cc} and $X(3872)$ exotic hadrons. Single range Gaussian potentials with the channel couplings to the isospin partners are constructed based on the empirical data within the pure hadronic-molecule picture. The momentum correlation functions of the $D^0 D^{*+}$, $D^+ D^{*0}$, $D^0 \bar{D}^{*0}$, and $D^+ D^{*-}$ pairs are computed with including the coupled-channel effects. We discuss how the nature of the exotic states are reflected in the behaviors of the correlation results.

1 Introduction

The study of various exotic resonances in heavy quark sectors has been one of the most interesting subjects in recent hadron physics [1–3]. The most extensively studied state is the $X(3872)$ lying just below the $D\bar{D}^*$ threshold, which is listed as $\chi_{c1}(3872)$ in the current PDG paper [4]. Ever since its first observation in 2003 [5], this exotic hadron has attracted huge interest of researchers and a bunch of the experimental and theoretical studies have been devoted to understand this state. Nevertheless, its nature still remains to be elucidated.

Recently, the LHCb Collaboration reported a clear signal of the doubly charmed tetraquark state T_{cc}^+ in the mass spectrum of $D^0 D^0 \pi^+$ [6,7]. Such exotic states with two heavy quarks and two light antiquarks are theoretically predicted with the quark model in Refs. [8,9] more than 30 years ago.

[a] e-mail: kamiya@hiskp.uni-bonn.de (corresponding author)

[b] e-mail: hyodo@tmu.ac.jp

[c] e-mail: ohnishi@yukawa.kyoto-u.ac.jp

In contrast to the $X(3872)$, this T_{cc} state is found in the genuine exotic channel, which requires at least four valence quark components ($cc\bar{u}\bar{d}$). Although the $X(3872)$ and T_{cc} are in different sectors, there is one similarity between them, i.e., the existence of a nearby two-meson threshold. Namely, the T_{cc} peak is also found just below the DD^* threshold. The proximity with the $D\bar{D}^*$ and DD^* thresholds would imply the molecular nature of these states. It should be noted, however, that the structure of X(3872) is still under debate. In the study of Ref. [10], it is shown that the contribution of the $c\bar{c}$ component is important by the analysis of the prompt production cross section. On the other hand, the enhancement of the production yield in AA collisions observed in CMS [11] seems to imply that $X(3872)$ contains a significant fraction of the hadronic molecule component [12]. In order to discriminate the possible structures of $X(3872)$, it is desirable to experimentally access the $D\bar{D}^*$ interaction. In the case where the hadronic molecule component is dominant in X(3872), the scattering length of $D\bar{D}^*$ is expected to agree with that from the weak binding relation [13–15], $a_0 \simeq -R_h = -\sqrt{-2\mu E_h}$ with μ and E_h being the reduced mass and the energy from the threshold. In the case where the $c\bar{c}$ and compact tetraquark components are significant, the scattering length will deviate from $-R_h$.

For the study of the near-threshold resonances, the femtoscopy using the two-particle momentum correlation function in high-energy collisions is a helpful technique because the correlation function is sensitive to the low-energy hadron interactions. With the femtoscopy, various interactions in the strangeness sector have been investigated theoretically [16–24] and experimentally [25–36]. It turns out that the source size dependence of the correlation function is useful to distinguish the existence or non-existence of hadronic bound states [22,23]. Recently, the $D^- p$ correlation function has been

measured by the ALICE collaboration [37], which paves the way to the femtoscopy in the charm sector.

In this study, we discuss the correlation functions of the $D D^*$ and $D \bar{D}^*$ channels towards the understanding of the nature of the T_{cc} and $X(3872)$ states. To this end, we construct one-range Gaussian potentials for the $D D^*$ and $D \bar{D}^*$ channels which reproduce the empirical information in these channels by assuming that the T_{cc} and $X(3872)$ are purely hadronic molecule states. Including the coupled-channel effects with the isospin partners and the decay channels, we compute the correlation functions. Deviation of the so predicted correlation function from the data to be measured in the near future signals the existence of non–hadronic-molecule components in T_{cc} and $X(3872)$.

This paper is organized as follows. In Sect. 2, we construct the $D D^*$ and $D \bar{D}^*$ potentials from the empirical data and summarize the method to calculate the correlation function with coupled-channel source effect. In Sect. 3, we show the results of the correlation functions of the $D^0 D^{*+}$, $D^+ D^{*0}$, $D^0 \bar{D}^{*0}$, and $D^+ D^{*-}$ channels and discuss how the exotic states can be studied in the future femtoscopy experiments. Section 4 is devoted to summarize this study.

2 Method

Let us first summarize the relevant channels which couple to the system of interest. For the T_{cc} and $X(3872)$ states, we cannot neglect the mass difference among the isospin multiplets, because the deviation of the eigenenergy from the threshold is comparable or smaller than the isospin breaking effect. The T_{cc} locates just below the $D^0 D^{*+}$ threshold, and it also couples to the $D^+ D^{*0}$ channel whose threshold lies slightly above that of the $D^0 D^{*+}$ channel. At energies lower than the T_{cc}, the three-body $D D \pi$ channels are open, which provide the finite decay width of T_{cc}. The $X(3872)$ lies just below the $\{D^0 \bar{D}^{*0}\} = (D^0 \bar{D}^{*0} + \bar{D}^0 D^{*0})/\sqrt{2}$ ($C = +$) threshold and couples also to the higher energy $\{D^+ D^{*-}\} = (D^+ D^{*-} + D^- D^{*+})/\sqrt{2}$ ($C = +$) channel. At much lower energies, the decay channels such as $\pi \pi J/\psi$ couple to the $X(3872)$. In the following, we explicitly treat the $D^0 D^{*+}$ and $D^+ D^{*0}$ channels for T_{cc} and $\{D^0 \bar{D}^{*0}\}$ and $\{D^+ D^{*-}\}$ channels for $X(3872)$, and the decay effect to the other channels are renormalized in the imaginary part of the potential. Thus, the Hamiltonian of the system is expressed by a 2×2 matrix in the channel basis.

Next, we construct the $D D^*$ and $D \bar{D}^*$ potentials. Assuming that the interaction is isospin symmetric, the strong interaction part of the coupled-channel potentials can be given by the $I = 0$ and $I = 1$ components as

$$V_{DD^*/D\bar{D}^*} = \frac{1}{2} \begin{pmatrix} V_{I=1} + V_{I=0} & V_{I=1} - V_{I=0} \\ V_{I=1} - V_{I=0} & V_{I=1} + V_{I=0} \end{pmatrix}, \quad (1)$$

where we assign channel $i = 1$ and 2 to $D^+ D^{*0}$ and $D^0 D^{*+}$ for the $D D^*$ system and $\{D^0 \bar{D}^{*0}\}$ and $\{D^+ D^{*-}\}$ for the $D \bar{D}^*$ system, respectively. Because the T_{cc} and $X(3872)$ couples to the $I = 0$ channel, we assume that the $I = 0$ component gives the dominant contribution, and set

$$V_{I=0} = V(r), \quad (2)$$
$$V_{I=1} = 0, \quad (3)$$

where $V(r)$ is a spherical Gaussian potential:

$$V(r) = V_0 \exp(-m^2 r^2), \quad (4)$$

where V_0 is the interaction strength and m is the parameter of the dimension of mass to control the range of the interaction. Here we use the charged (isospin averaged) pion mass $m_{\pi^\pm}$ (m_π) for the $D D^*$ ($D \bar{D}^*$) interactions because the lightest exchangeable meson, pion, determines the interaction range (see 1 for the different choice of m and the finite $V_{I=1}$ case in the $D \bar{D}^*$ channel). Thus, in this formulation, we are left with a single parameter V_0 for each $D D^*/D \bar{D}^*$ potential. Note that V_0 takes a complex number, in order to express the decay effects into the lower energy channels. While the $D D^*$ potential is free from the Coulomb interaction, for the $\{D^+ D^{*-}\}$ channel we should include the Coulomb force:

$$V_{D\bar{D}^*}^c(r) = \begin{pmatrix} 0 & 0 \\ 0 & -\alpha/r \end{pmatrix}, \quad (5)$$

with the fine structure constant α. This potential is added to Eq. (1) for the $D \bar{D}^*$ potential.

Here we determine the potential strength V_0 so as to reproduce the empirical data for these systems. For the $D D^*$ potential, we use the scattering length $a_0^{D^0 D^{*+}} = -7.16 + i 1.85$ fm, given in the experimental analysis in Ref. [7].[1] For the $D \bar{D}^*$ potential, we use the scattering length $a_0^{\{D^0 \bar{D}^{*0}\}} = -4.23 + i 3.95$ fm which is determined by the eigenenergy $E_h = -0.04 - i 0.60$ MeV in PDG [4] measured from the $D^0 \bar{D}^{*0}$ threshold, as $a_0^{\{D^0 \bar{D}^{*0}\}} = -i/\sqrt{2\mu E_h}$ with the reduced mass μ. We notice that these scattering lengths have a much larger magnitude than the typical length scale of the strong interaction ~ 1 fm. The obtained potential strengths are summarized in Table 1. For the later use, the scattering lengths of the higher channels ($D^+ D^{*0}$ and $\{D^+ D^{*-}\}$) calculated with the same potentials are also listed. Our potential model looks too simple to describe the mechanism to produce the T_{cc} and $X(3872)$ from the $D D^*$ and $D \bar{D}^*$ interaction. It should be noted that, however, the correlation function at small relative momenta is mainly determined

---

[1] Here we use the the high-energy physics convention for the scattering length where the positive (negative) real value corresponds to the weakly attractive (repulsive or strongly attractive) interaction.

Table 1 Strength parameters V_0 for the DD^* and $D\bar{D}^*$ potentials and the scattering lengths in the DD^* and $D\bar{D}^*$ channels

DD^*	V_0 [MeV]	$a_0^{D^0 D^{*+}}$ [fm]	$a_0^{D^+ D^{*0}}$ [fm]
	$-36.569 - i1.243$	$-7.16 + i1.85$	$-1.75 + i1.82$
$\{D\bar{D}^*\}$	V_0 [MeV]	$a_0^{\{D^0 \bar{D}^{*0}\}}$ [fm]	$a_0^{\{D^+ D^{*-}\}}$ [fm]
	$-42.116 - i6.057$	$-4.23 + i3.95$	$-0.39 + i1.49$

The scattering lengths of the lower channels (third column) are the empirical inputs

by the scattering lengths and the energy from the threshold together with the source size. Then it is decisive to obtain the coupled-channel wave function in the low energy region with the potentials having appropriate scattering lengths. To this end, our potential model determined directly from the empirical data is useful to discuss the behavior of the DD^* and $D\bar{D}^*$ correlation functions without suffering from the detailed model dependence. Note that all these calculations are performed in the coupled-channel scheme.

To calculate the correlation functions $C(q)$ with the coupled-channel effects, we employ the Koonin-Pratt-Lednicky-Lyuboshitz-Lyuboshitz formula (KPLLL) formula [21,24,38] given by

$$C(q) = \int d^3 r \sum_{i=1}^{2} \omega_i S_i(r) |\Psi_i^{(-)}(q; r)|^2, \qquad (6)$$

where the wave function $\Psi_i^{(-)}$ in the i-th channel is written as a function of the relative coordinate r, with imposing the outgoing boundary condition on the measured channel. We consider the small momentum region and assume that only the s-wave component of the wave function $\Psi_i^{(-)}$ is modified by the strong interaction. The wave function is calculated by solving the Schrödinger equation with the hermite conjugated potential $V^\dagger$, which gives the appropriate boundary condition for the eliminated decay channels (See 1). We adopt a common static Gaussian source function for all the channels $S_i(r) = \exp(-r^2/4R^2)/(4\pi R^2)^{3/2}$ with the source size R, and the weight factor ω_i is taken as unity for all channels. The weight factor ω_i represents the ratio of the pair production yield in the ith channel with respect to the measured channel. Since we only include the coupled-channel effect of the isospin partners, they are considered to have the equivalent emitting source. The source size R ranges from ~ 1 fm for the high-multiplicity events in pp collisions to $\sim (5-6)$ fm for the central PbPb collisions.

While we construct the $D\bar{D}^*$ potential in the charge conjugation $C = +$ combination which couples to the $X(3872)$, the experimental measurement of the correlation function will be done with fixed charge states, i.e., either $D^0 \bar{D}^{*0}$ or $\bar{D}^0 D^{*0}$. To obtain the correlation functions of the fixed charge states, the correlation functions in the $C = -$ sector are also needed to take an average of the $C = +$ and $C = -$ contributions. In this exploratory study, we assume that the $C = -$ interaction

is small and can be neglected with respect to the dominant $C = +$ contribution. In this case, we obtain the experimentally accessible correlation functions from the correlation function calculated by the $C = +$ potential as

$$C_{D^0 \bar{D}^{*0}} = C_{\bar{D}^0 D^{*0}} = \frac{1}{2} \left(C_{\{D^0 \bar{D}^{*0}\}} + 1 \right), \qquad (7)$$

$$C_{D^+ D^{*-}} = C_{D^- D^{*+}} = \frac{1}{2} \left(C_{\{D^+ D^{*-}\}} + C_{\text{pure Coul.}} \right), \qquad (8)$$

where $C_{\text{pure Coul.}}$ is calculated only with the Coulomb interaction by switching off the strong interaction contribution.

3 Results

Now we calculate the correlation functions with the constructed potentials. First we show the DD^* sector coupled with the T_{cc} state. The correlation function of the $D^0 D^{*+}$ and the $D^+ D^{*0}$ pairs with source sizes $R = 1, 2, 3,$ and 5 fm are shown in Fig. 1. We can see that the source size dependence typical to the system with a shallow bound state for both correlation functions; the enhancement in the small source case turns to the suppression for the large source case [24]. The stronger correlation is found in the $D^0 D^{*+}$ channel, whose threshold is closer to the T_{cc} pole. The cusp structure is seen at the $D^+ D^{*0}$ threshold ($q \simeq 52$ MeV/c) in the $D^0 D^{*+}$ correlation, while the strength is not very prominent. The $D^0 D^{*+}$ correlation behavior is typical to the dynamically generated state with the large scattering length [24]. If T_{cc} is not originated in the D-D interaction and the scattering lengths ($a_0^{D^0 D^{*+}}$ and $a_0^{D^+ D^{*0}}$) deviate from $-R_h$, it is expected that both correlation function shows the weaker signal and source size dependence.

Next we show the results of the $D\bar{D}^*$ correlation function coupled with the $X(3872)$ in Fig. 2. Here we plot the correlation functions of the fixed charges states in Eqs. (7) and (8) which can be compared with the experimental measurements. The characteristic strong source size dependence with the shallow bound state is found in $C_{D^0 \bar{D}^{*0}}$. We can also see the cusp structure at the $D^+ D^{*-}$ threshold ($q \simeq 126$ MeV/c). The cusp structure is more prominent for the smaller source case. This is because the coupled-channel source effect by the $D^+ D^{*-}$ channel is stronger for the smaller source case
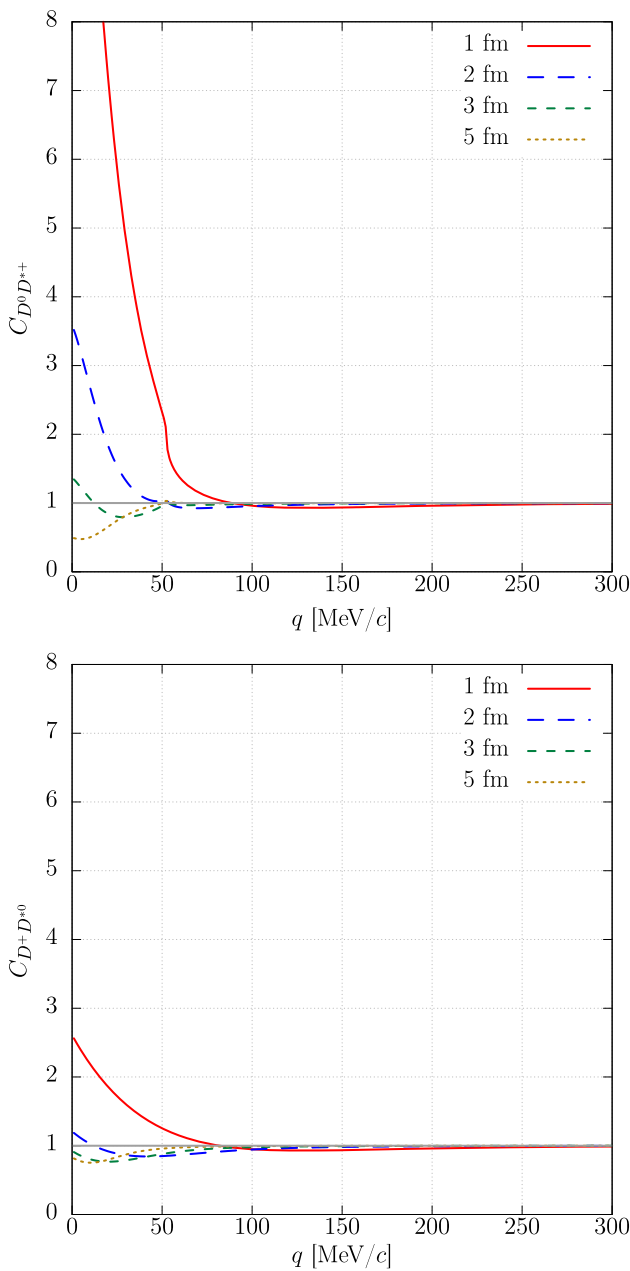
Fig. 1 The correlation functions of the $D^0 D^{*+}$ (top) and $D^+ D^{*0}$ (bottom) pair with the source size $R = 1, 2, 3$, and 5 fm
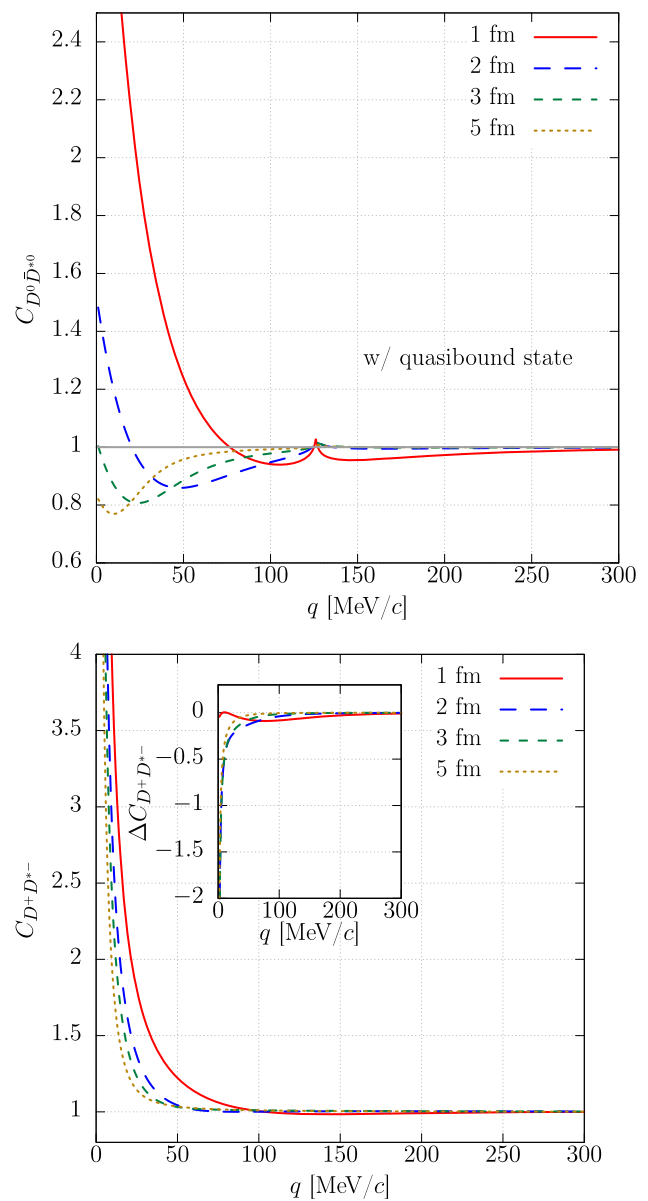

Fig. 2 The correlation functions of the $D^0 \bar{D}^{*0}$ (top) and $D^+ D^{*-}$ (bottom) pair with the source size $R = 1, 2, 3$, and 5 fm. For $D^+ D^{*-}$ pair, the difference from the pure Coulomb case ΔC is shown in sub figure

[23]. On the other hand, due to the attractive Coulomb force, the $C_{D^+ D^{*-}}$ correlations show a strong enhancement at small q. To extract the contribution by the strong interaction, we show the difference from the pure Coulomb case $\Delta C = C_{D^+ D^{*-}} - C_{\text{pure Coul.}}$. We can see that the effect of the strong interaction emerges mainly as the suppression compared to the pure Coulomb case. However, the deviation $|\Delta C|$ is less than 0.2 for the momentum region $q > 50$ MeV/c. Thus, the correlation of $D^+ D^{*-}$ pair is expected to be dominated by the Coulomb contribution.

Up to here, we have assumed that $X(3872)$ is the quasi-bound state below the $D\bar{D}^*$ threshold. Another possibility is that the $X(3872)$ pole emerges above the threshold energy in the unphysical Riemann sheet. In this case, the real part of $a_0^{\{D^0 \bar{D}^{*0}\}}$ is positive. We find that when we weaken the real part of the V_0 and take $V_0 = -32.000 - i6.057$ MeV, $a_0^{\{D^0 \bar{D}^{*0}\}} = 2.30 + i4.00$ fm and $a_0^{\{D^+ \bar{D}^{*-}\}} = 0.19 + i1.47$ fm. We performed the calculation in the same manner and obtained the $D^0 \bar{D}^{*0}$ correlation function with the weakened potential as shown in Fig. 3. We see that the correlation function shows the source size dependence different from Fig. 2.
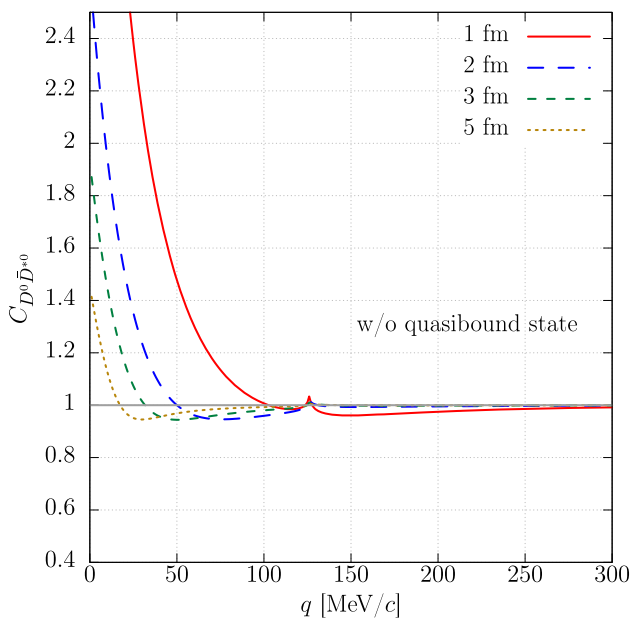
Fig. 3 The $D^0\bar{D}^{*0}$ correlation functions calculated with the weakened interaction $V_0 = -32.000 - i6.057$ MeV (thick line) where the quasibound state does not appear. The scattering length is obtained as $a_0^{\{D^0\bar{D}^{*0}\}} = 2.30 + i4.00$ fm

Due to the large absolute value of the $a_0^{\{D^0\bar{D}^{*0}\}}$, $C_{D^0\bar{D}^{*0}}$ from the small source shows the strong enhancement, which is similar to the quasibound case. However, $C_{D^0\bar{D}^{*0}}$ from the large source does not show the clear dip structure unlike Fig. 2. Thus, even though the pole is originated in the D-$\bar{D}^*$ interaction, the $D^0\bar{D}^{*0}$ correlation function shows the different source size dependence depending on the pole position of $X(3872)$. On the other hand, D^+D^{*-} pair shows the same behavior with Fig. 2 due to the small $a_0^{\{D^+D^{*-}\}}$, so we omit the result of $C_{D^+D^{*-}}$.

In this study, we used the empirically determined scattering lengths as input to calculate the correlation functions. Given the correlation data obtained from the precise future measurement, we can independently determine the scattering lengths a_0 because the correlation functions are sensitive to the low-energy interaction. According to the Weinberg's weak-binding relation [13–15], the compositeness, which is defined as the probability of finding molecular state in the eigenstate, is directly related to the ratio of the a_0/R_h where R_h is the length scale determined with the eigenenergy E_h as $R_h = 1/\sqrt{-2\mu E_h}$. Thus, combined with the information of the pole position, to measure the these correlation functions leads to understand the nature of T_{cc} and $X(3872)$ states.

4 Summary

We have studied the correlation functions of the DD^* and $D\bar{D}^*$ pairs for the purpose of the investigation of the T_{cc} and

$X(3872)$ exotic states. With the assumption of the molecular nature of these states, one-range Gaussian potentials are constructed for the DD^* and $D\bar{D}^*$ channels from the empirical data, the scattering length given in the experimental analysis [7] for DD^* and the eigenenergy of $X(3872)$ [4] for $D\bar{D}^*$. Due to the large scattering lengths, the calculated correlation functions in the lower channels (D^0D^{*+} and $D^0\bar{D}^{*0}$), which are closer to the exotic states, show the characteristic behavior of the bound state below the threshold. On the other hand, the correlation function of the D^+D^{*0} channel shows less prominent behavior due to the energy difference from the T_{cc} pole, and the correlation in the D^+D^{*-} channel is mainly caused by the Coulomb interaction. To extract these characteristic behaviors, the high resolution data given by the statistical events from the different collisions systems is required. According to Refs. [39,40], the ALICE 3 upgrade with the large acceptance and the high luminosity provides us the great resolution for the DD^* and $D\bar{D}^*$ correlation data from both different colliding systems (pp and PbPb), which is enough to see the characteristic behavior. Given the successful measurement of the D^-p correlation function by the ALICE collaboration [37], we expect that the measurements of the DD^* and $D\bar{D}^*$ correlations in future will bring new insights of the exotic hadrons from the viewpoint of the femtoscopy.

In this study, we have introduced the potentials in the channels that couple to the exotic states (isospin $I = 0$ and charge conjugation $C = +$), and have neglected the interactions in the other channels. This is because the existence of near-threshold states implies the strong interaction, which is considered to give the dominant contribution for the correlation function. For more quantitative discussion of the correlation functions, these subleading effects should also be considered. In particular, the cusp structure may be sensitive to the isospin $I = 1$ interaction, because the coupling between the isospin partners are given by the difference of the two isospin components. The $D\bar{D}^*$ interaction in the $C = -$ sector is still unclear at this moment, but the neutral partner of $Z_c(3900)$ [41] may play an important role in this channel. These effect should be discussed in the future studies.

Appendix A: Outgoing boundary condition for the optical complex potential

The wave function for the KPLLL formula (6) must satisfy the outgoing boundary condition where the flux of the outgoing wave of the reference channel is normalized to be unity. On the other hand, the complex optical potentials are constructed based on the scattering problem with the incoming boundary condition where the flux of the incoming wave is normalized. This boundary condition is applied to the integrated channels, whose coupling to referenced channels (D^+D^{*0} and D^0D^{*+} in the case of DD^* sector) give the imaginary part of the potential. Thus, we cannot obtain the correct wave function ψ by solving the Schrödinger equation

$$H\psi = [H_0 + V]\psi = E\psi, \tag{A.1}$$

with the boundary condition only with the referenced channels.

We claim that we can just take the hermite conjugate of the potential V and solve the Schrödinger equation in order to obtain the wave function which satisfies the boundary conditions for all the channels,

$$[H_0 + V^\dagger]\psi = E\psi, \tag{A.2}$$

with the outgoing boundary condition.

Taking the hermite conjugate of the potential V corresponds to consider the time reversal of the system. This can be understood as follows. Let us consider the two channel scattering problem with spinless particles where channel 1 (2) has higher threshold energy and is measured (lower threshold energy and is not measured). The Hamiltonian for this system is given as

$$H = \begin{pmatrix} H_{11} & H_{12} \\ H_{21} & H_{22} \end{pmatrix} = \begin{pmatrix} H_{11}^0 + V_{11} & V_{12} \\ V_{21} & H_{22}^0 + V_{22} \end{pmatrix}, \tag{A.3}$$

where H_{ij}^0 and V_{ij} are the free Hamiltonian and the interaction potential, respectively. The Lippmann-Schwinger equation for the T matrix is given as

$$T = V + VG^0T, \tag{A.4}$$
$$G^0 = \text{diag.}(G_1^0, G_2^0), \tag{A.5}$$

with the free propagator

$$G_i^0(z) = (z - H_{ii}^0)^{-1}. \tag{A.6}$$

With the Feshbach projection [42,43] for channel 2, the Lippmann-Schwinger equation for channel 1 can be written with the effective potential V_{eff} as

$$T_{11}(z) = V_{\text{eff}}(z) + V_{\text{eff}}(z)G_1^0(z)T_{11}(z), \tag{A.7}$$
$$V_{\text{eff}}(z) = V_{11} + V_{12}G_2(z)V_{21}, \tag{A.8}$$

where $G_i(z)$ is the full propagator given as

$$G_i(z) = (z - H_{ii})^{-1}. \tag{A.9}$$

The contour of the time integration of $G_i^{(0)}(z)$ can be chosen by taking $z \to E + i\epsilon$ for the scattering problem. On the other hand, that of the time-reversed system can be given as $z \to E - i\epsilon$. This effective potential is complex due to the pole term included in $G_2(E - i\epsilon)$. Then the effective potential in the time reversed system is given as

$$\begin{aligned} V_{\text{eff}}(E - i\epsilon) &= V_{11} + V_{12}G_2(E - i\epsilon)V_{21} \\ &= V_{11}^\dagger + V_{21}^\dagger G_2^\dagger(E + i\epsilon)V_{12}^\dagger \\ &= [V_{11} + V_{12}G_2(E + i\epsilon)V_{21}]^\dagger \\ &= V_{\text{eff}}^\dagger(E + i\epsilon). \end{aligned} \tag{A.10}$$

Here we assumed that the full Hamiltonian is hermitian and the potential V is real. Thus, the hermite conjugated effective potential corresponds to that in the time reversed system. Remembering that the time reversal operator T acts on the wave function as $T\psi = \psi^*$ [44], the system obtained from Eq. (A.2) with the outgoing boundary condition corresponds to the time-reversed system written with Eq. (A.1) with incoming boundary condition.

The imaginary part of the optical potential causes the suppression or the enhancement of the wave function component of the referenced channel depending on its sign. In the scattering problem of the coupled-channel system, the asymptotic form of the s-wave component of the scattering wave function of channel 1 is given with the S matrix component as

$$\psi_1(q; r) \to \frac{1}{2iqr}\left(e^{-iqr} - \mathcal{S}_{11}e^{iqr}\right). \tag{A.11}$$

Table 2 Strength parameters V_0 for the $D\bar{D}^*$ potential and the scattering lengths of D^+D^{*-} channel with different potential assumptions for the range parameter m and the $I = 1$ potential $V_{I=1}$

m	m_ρ	m_π	m_π	m_π
$V_{I=1}$	0	Re $V_{I=0}/3$	$-$Re $V_{I=0}/3$	0
V_0 [MeV]	$-924.58 - i16.92$	$-40.088 - i6.998$	$-43.257 - i5.372$	$-42.116 - i6.057$
$a_0^{\{D^+D^{*-}\}}$ [fm]	$-0.73 + i0.73$	$0.45 + i4.45$	$-1.01 + i0.93$	$-0.39 + i1.49$

The case with the original assumption is shown in the fifth column

Due to the coupling to channel 2, the absolute value of the S matrix component S_{11} is less than unity, which leads the reduced outgoing wave (e^{iqr}) compared to the normalized incoming wave (e^{-iqr}). When we use the complex optical potential V with negative imaginary part, this reduction of the wave function is caused by the imaginary part of the potential. On the other hand, the outgoing boundary condition, which is used for the correlation study, is given as

$$\psi_1(q; r) \to \frac{1}{2iqr}\left(e^{iqr} - \mathcal{S}_{11}^\dagger e^{-iqr}\right). \tag{A.12}$$

In this case, the flux of the outgoing wave (1) is larger than that of the incoming wave ($|\mathcal{S}_{11}^\dagger|$). This is because the wave function of channel 2 flows into channel 1 by the coupling potential to give the normalized outgoing wave. When we use the hermite conjugated optical potential $V^\dagger$ with positive imaginary part, its imaginary part causes the enhancement of the channel 1 component.

In summary, when we employ the complex optical potential constructed for the ordinarily scattering problem, the wave function for the KPLLL formula (6) can be obtained by solving Eq. (A.2) with hermite conjugated potential $V^\dagger$ with the outgoing boundary condition. This is because to take the hermite conjugate of the potential V corresponds to consider the time reversal of the system, which turns the incoming boundary condition introduced in the construction process of the potential to the outgoing boundary condition. We also note that the resulting wave function can also be obtained by solving Eq. (A.1) with the (standard) incoming boundary condition and taking the complex conjugate of the wave function.

Appendix B: Interaction dependence of $D\bar{D}^*$ correlation function

In the main text, we studied the $D\bar{D}^*$ correlation functions with the assumptions that the range of the interaction is governed by the pion exchange and that the $I = 0$ interaction gives the dominant contribution. In this appendix, we perform further calculations with different assumptions on the $D\bar{D}^*$ interaction so that how the behavior of the correlation
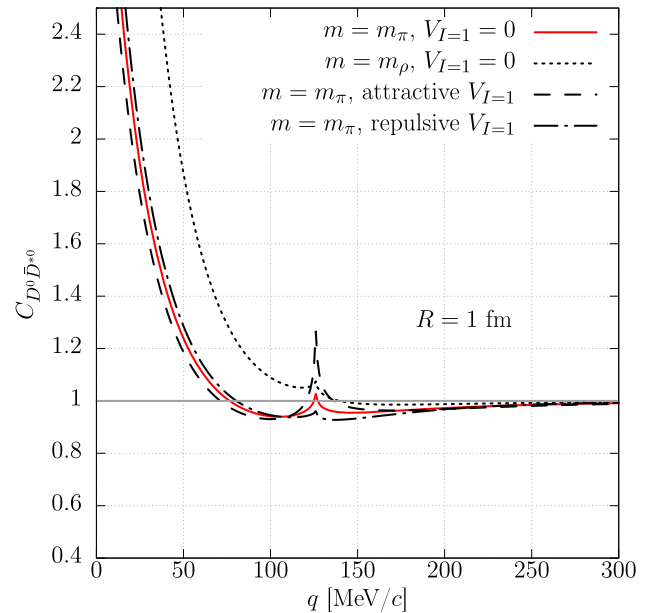

Fig. 4 The $D^0\bar{D}^{*0}$ correlation function calculated with different potential assumptions. The case where the ρ meson mass is used for the range parameter is shown by the dotted line. The case where the attractive (repulsive) $I = 1$ potential is shown by dashed (dash-dotted) line. The correlation calculated with the original assumption is shown by the solid line for the comparison

functions depends on these assumptions. Because we find no significant change of the D^+D^{*-} correlation, here we only present the result of the neutral $D^0\bar{D}^{*0}$ correlation function.

First we consider the different interaction range of the potential. Although the natural underlying mechanism of the $D\bar{D}^*$ interaction is the pion exchange, as a conservative estimate, we examine the case where the mass of the ρ meson m_ρ is employed as m in Eq. (4), which gives a much shorter interaction range compared to that of the π exchange. With this assumption, we fitted the V_0 again so that the calculated scattering length reproduces the empirical value of $a_0^{\{D^0\bar{D}^{*0}\}} = -4.23 + i3.95$ fm. The obtained potential strength and the calculated scattering length of D^+D^{*-} channel are shown in Table 2. Because the potential reproduces the same scattering length, the change of the wave function emerges mainly in the small r but not in the asymptotic region. Thus, we only plot the correlation function with

$R = 1$ fm source case (dotted line) in Fig. 4, which is most affected by the change of the inner part of the wave function. From this figure, we can see that the $C_{D^0\bar{D}^{*0}}$ is more enhanced at small q region than the case with $m = m_\pi$ (solid line), which we call the original case in this appendix. We also checked that the behavior of the source size dependence discussed in Sect. 3 is not affected by the change of m. In short, the difference of the interaction range only appears as the strength of the enhancement of $D^0\bar{D}^{*0}$ channel for the small source.

Next we consider the case with the finite $I = 1$ interaction $V_{I=1}$. Here we examine both cases of attractive $V_{I=1}$ and repulsive $V_{I=1}$. For the strength, we expect the strength of $V_{I=1}$ to be 1/3 of that of $V_{I=0}$ because the π exchange interaction gives the factor of $I \cdot I'$ with the isospin of D meson I and that of $\bar{D}^*$ meson I', which leads to $V_{I=0}/V_{I=1} = -3$. Based on this observation, we assume that the $V_{I=1}$ is given as $V_{I=1} = \mathrm{Re}\, V_{I=0}/3$ ($V_{I=1} = -\mathrm{Re}\, V_{I=0}/3$) for the attractive (repulsive) case. Here we use the real potential for $V_{I=1}$ for the simplicity. With this assumption, the $I = 0$ and $I = 1$ potential is given by the potential strength parameter V_0 as

$$V_{I=0} = V_0 \exp(-m_\pi^2 r^2), \tag{B.13}$$

$$V_{I=1} = \pm\frac{1}{3}\mathrm{Re}\, V_0 \exp(-m_\pi^2 r^2). \tag{B.14}$$

As in the same procedure, V_0 is determined as shown in Table 2. Because the quasibound pole corresponding to the $X(3872)$ state, which is strongly related to the $D^0\bar{D}^{*0}$ scattering length, is generated by the $I = 0$ component, the change of the strength parameter V_0 is small. On the other hand, we find that the value of the $\{D^+D^{*-}\}$ scattering length is sensitive to the assumption of $V_{I=1}$. This is because the value of $a_0^{\{D^+D^{*-}\}}$ is affected by the pole in the unphysical Riemann sheet, which would have appeared as a quasibound state below the D^+D^{*-} threshold if the attractive interaction had been strong enough. The added attractive (repulsive) $V_{I=1}$ in Eq. (B.14) bring its position closer to (farther from) the D^+D^{*-} threshold, which affects the value of $a_0^{\{D^+D^{*-}\}}$. As shown in Fig. 4, compared with the original case, the $D^0\bar{D}^{*0}$ correlation function in the low momentum region ($q < 100$ MeV) is almost unchanged while the D^+D^{*-} cusp structure is enhanced (suppressed) in the case of attractive (repulsive) $V_{I=1}$. This enhancement (suppression) of the cusp is caused by the strengthened (weakened) imaginary part of the D^+D^{*-} scattering length, which reflects the coupling strength to the coupled-channels. Thus, by measuring the cusp structure with the precise experiment, the detailed isospin dependence of the interaction can be investigated.

References

1. A. Hosaka, T. Iijima, K. Miyabayashi, Y. Sakai, S. Yasui, PTEP **2016**, 062C01-6 (2016)
2. F.K. Guo, C. Hanhart, U.G. Meißner, Q. Wang, Q. Zhao, B.S. Zou, Rev. Mod. Phys. **90**(1), 015004 (2018)
3. N. Brambilla, S. Eidelman, C. Hanhart, A. Nefediev, C.P. Shen, C.E. Thomas, A. Vairo, C.Z. Yuan, Phys. Rept. **873**, 1–154 (2020)
4. P.A. Zyle et al., PTEP **20208**, 083C01 (2020). (**Particle Data Group**)
5. S.K.C. Belle et al., Phys. Rev. Lett. **91**, 262001 (2003)
6. LHCb Collaboration. Nat. Phys. **18**, 751–754 (2022)
7. LHCb collaboration. Nat. Commun **13**, 3351 (2022)
8. J.I. Ballot, J.M. Richard, Phys. Lett. B **123**, 449–451 (1983)
9. S. Zouzou, B. Silvestre-Brac, C. Gignoux, J.M. Richard, Z. Phys. C **30**, 457 (1986)
10. C. Bignamini, B. Grinstein, F. Piccinini, A.D. Polosa, C. Sabelli, Phys. Rev. Lett. **103**, 162001 (2009)
11. A.M. Sirunyan et al., CMS. Phys. Rev. Lett. **128**(3), 032001 (2022)
12. S. Cho et al., ExHIC. Prog. Part. Nucl. Phys. **95**, 279–322 (2017)
13. S. Weinberg, Phys. Rev. **137**, B672 (1965)
14. Y. Kamiya, T. Hyodo, Phys. Rev. C **93**, 035203 (2016)
15. Y. Kamiya, T. Hyodo, PTEP **2017**, 023D02 (2017)
16. K. Morita, T. Furumoto, A. Ohnishi, Phys. Rev. C **91**, 024916 (2015)
17. A. Ohnishi, K. Morita, K. Miyahara, T. Hyodo, Nucl. Phys. A **954**, 294 (2016)
18. K. Morita, A. Ohnishi, F. Etminan, T. Hatsuda, Phys. Rev. C **94**, 031901 (2016)
19. T. Hatsuda, K. Morita, A. Ohnishi, K. Sasaki, Nucl. Phys. A **967**, 856 (2017)
20. D.L. Mihaylov et al., Eur. Phys. J. C **78**, 394 (2018)
21. J. Haidenbauer, Nucl. Phys. A **981**, 1 (2019)
22. K. Morita et al., Phys. Rev. C **101**, 015201 (2020)
23. Y. Kamiya, T. Hyodo, K. Morita, A. Ohnishi, W. Weise, Phys. Rev. Lett. **124**, 132501 (2020)
24. Y. Kamiya, K. Sasaki, T. Fukui, T. Hyodo, K. Morita, K. Ogata, A. Ohnishi, T. Hatsuda, Phys. Rev. C **105**(1), 014915 (2022)
25. L. Adamczyk et al., STAR. Phys. Rev. Lett. **114**(2), 022301 (2015)
26. S. Acharya et al., ALICE. Phys. Lett. B **774**, 64–77 (2017)
27. J. Adam et al., STAR. Phys. Lett. B **790**, 490–497 (2019)
28. S. Acharya et al., ALICE. Phys. Rev. C **99**(2), 024001 (2019)
29. S. Acharya et al., ALICE. Phys. Rev. Lett. **123**(11), 112002 (2019)
30. S. Acharya et al., ALICE. Phys. Lett. B **805**, 135419 (2020)
31. S. Acharya et al., ALICE. Phys. Lett. B **797**, 134822 (2019)
32. S. Acharya et al., ALICE. Phys. Rev. Lett. **124**(9), 092301 (2020)
33. S. Acharya et al., ALICE. Nature **588**, 232–238 (2020)
34. S. Acharya et al., ALICE. Phys. Lett. B **822**, 136708 (2021)
35. S. Acharya et al., ALICE. Phys. Rev. Lett. **127**(17), 172301 (2021)
36. L. Fabbietti, V. Mantovani Sarti, O. Vazquez Doce, Ann. Rev. Nucl. Part. Sci. **71**, 377–402 (2021)
37. S. Acharya et al., [ALICE], [arXiv:2201.05352 [nucl-ex]] (2022)
38. R. Lednicky, V.V. Lyuboshits, V.L. Lyuboshits, Phys. Atomic Nuclei **61**, 2950 (1998)
39. ALICE collaboration, CERN-LHCC-2022-009. https://cds.cern.ch/record/2803563 (2022)
40. F. Grosa et al., (ALICE Collaboration), talk at Quark Matter. https://indico.cern.ch/event/895086/contributions/4715876/ (2022)
41. M. Ablikim et al., BESIII. Phys. Rev. Lett. **115**(11), 112003 (2015)
42. H. Feshbach, Ann. Phys. **5**, 357–390 (1958)
43. H. Feshbach, Ann. Phys. **19**, 287–313 (1962)
44. J.R. Taylor, *Scattering Theory: The Quantum Theory on Nonrelativistic Collisions* (Wiley, New York, 1972)